INTERNATIONAL JOURNAL OF INTELLIGENT CONTROL AND SYSTEMS
VOL. 13, NO. 4, DECEMBER 2008, 242-250

Singular Value Decomposition Filter: an Effective Method to Enhance the SwissRanger SR-3000's Range Images

GuruPrasad M. HEGDE and Cang YE

Abstract – **This paper presents the research results on the enhancement of the SwissRanger SR-3000's range images by a Singular Value Decomposition (SVD) filtering method. The image enhancement is performed by converting a conventional range image into an enhanced range image where each pixel's intensity embodies the surface normal and depth information of the corresponding pixel in the original image. This range image representation makes an object's edges distinctive. But it corrupts the object's surfaces due to the noise in the range data. We propose a filtering method based on the SVD to alleviate the surface corruption and preserve the edges. The efficacy of the proposed method is validated by numerous experiments in various environments.**

***Index Terms*—Singular Value Decomposition filter, normal-enhanced range image, flash LADAR.**

I. INTRODUCTION

Range image segmentation is an important research problem in range data processing. For autonomous navigation, a set of properly segmented range data makes it possible for a mobile robot to detect obstacles and ground level; and even recognize objects. In many of the existing projects, Laser Detection and Ranging (LADAR) [1] and stereovision systems [2] are used to collect 3D range data of the environments. A LADAR system, also called Laser Rangefinder (LRF), profiles its environment by using a rotating mirror to scan a laser beam. Such a mechanism results in a low range data throughput. A LADAR-based 3D mapping system is good for map-building with a stationary platform. If a mobile platform is used, a highly accurate Inertial Measurement Unit (IMU) is required to register each laser scan into a 3D map. Such a system may be prohibitively costly and therefore unsuitable for many mobile robotic applications. In addition, A LADAR system is bulky and thus cannot be used in a small-sized mobile platform. A stereovision system determines depth values using disparity images. It needs to match a pixel in one camera to that in another camera, and triangulates its depth information. This operating principle limits its use in feature-rich environments. Also, a stereovision system is sensitive to illumination and has low range resolution and accuracy for a distant object.

Recently a new-class of 3D ranging sensors have been developed by several groups [3], [4]. These devices are commonly referred to as "Flash LADAR" [5], [6], [7]. They illuminate the entire scene by a modulated light source. Each cell of the imaging sensor can determine the time-of-flight of the modulated signal and thus the depth information of the detected object. These devices do not require a scanning mechanism and can provide dense data points at a high frame rate. Therefore, they are ideal for 3D map-building on a moving platform. This paper investigates the use of a Flash LADAR—the SwissRanger SR-3000 [8]—for mobile robot navigation. Figure 1(a) depicts the miniature SR-3000 sensor. A detailed description of the sensor will be given in Section II. We plan to use this sensor for 3D mapping and autonomous navigation. Figure 1(b) is a snapshot taken from our experiment to calibrate the sensor using the LRF's data.

As an active vision sensor, the SR-3000 has an apparent advantage over a stereovision system: it works very well in featureless environment. Figure 2 demonstrates that SR-3000 outperforms a stereovision system in a normal indoor environment. Figure 2(a) is a video image from the stereovision system's left camera and Fig. 2(b) is the grey-encoded range data. We can observe that range data of those areas without distinctive features, such as the wall and human subject, are missing. Figure 2(d) illustrates that SR-3000 obtains all range data for all objects in its field of view (i.e., no missing data). Capturing all range data of the environment is an essential capability for an imaging sensor for robotic navigation.

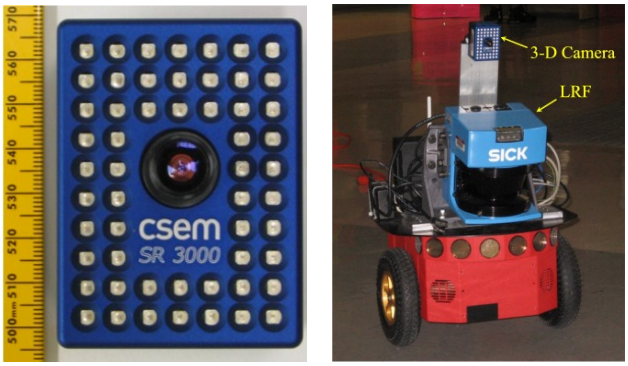

(a) The SR-3000 sensor (b) SR-3000 on the robot

Fig.1 SR-3000 and LRF mounted on the Pioneer P3-DX robot: SR-3000 is much smaller in size.

As the sensing technology is in its early stage, the data of the current SR-3000 sensor has relatively large range measurement errors (much bigger than that of a LADAR [9]) and the errors increase with range values. Both the sensor's random noise (e.g., thermal noise and photon short noise) and the environmental factors (e.g., surface reflectivity) can produce range errors. The large range errors may cause problems in range data processing. Kim *et al.* [22] remove SR-3000's random noise by Gaussian and median filtering, and model the systematic bias as a function of rigid misalignment, ray directional misalignment and distance error along ray. They first compute the intrinsics and extrinsics of

This work was funded by NASA through Arkansas Space Grant Consortium under grant number UALR16800 and a NASA EPSCOR Research Infrastructure Development award.

C. Ye is with Department of Applied Science, University of Arkansas at Little Rock, 2801 S. University Ave, Little Rock, AR 72204, USA (e-mail: cxye@ualr.edu). GuruPrasad M. Hegde is with the same department (e-mail: gmhegde@ualr.edu).

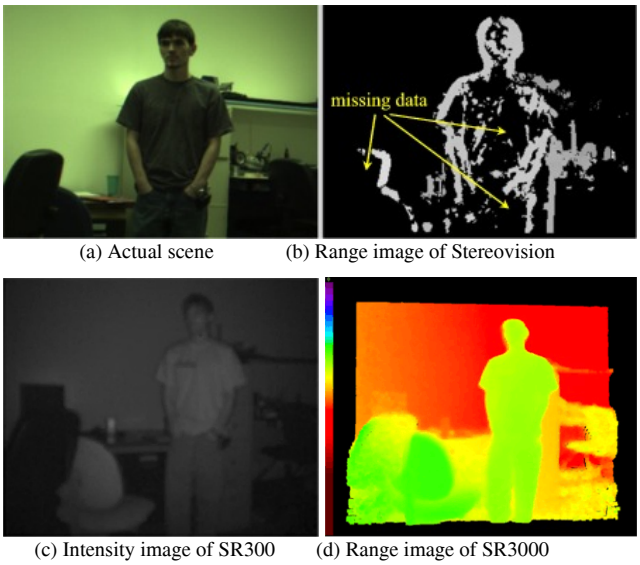

(a) Actual scene (b) Range image of Stereovision

(c) Intensity image of SR300 (d) Range image of SR3000

Fig. 2 Stereovision vs SR-3000: Large amount of range data are missing in the stereovision's range image while there is no missing data in that of SR-3000.

SR-3000 and a video camera by using a checkerboard and the MATLAB calibration toolbox. The 3-D data points captured by the video camera with the checkerboard at different positions are used as ground truth data to calibrate SR-3000. The calibration is performed by computing the rigid transformation that minimizes the misalignment of the SR-3000 data points with the ground truth data, the directional compensation, and the correction of distance along ray. In spite of a significant improvement of accuracy reported in the paper, the calibration method is only valid for a fixed set of recording conditions. In addition, the calibration is performed pixel by pixel which might not be suitable for real-time implementation.

In the literature, surface normal has been used to enhance a range image (in particular the edges) and thus facilitate range image segmentation [17], [18]. However, the normal-based approach is very sensitive to noise in range data and may corrupt the object surfaces while enhancing the edges. It then becomes necessary to study the effect of the range noise on the Normal-Enhanced Range Image (NERI) and to develop a method to alleviate the ill effect.

In this work, we propose a filtering method based on the Singular Value Decomposition (SVD) to reduce the surface corruption but preserve the edge information. In our study the level of surface corruption is qualitatively evaluated by observing the NERI and its edge image. The rest of this paper is organized as follows: In Section II we briefly describe the SR-3000 range sensor. In Section III we explain the principle of the SVD filtering method in noise reduction. In Section IV and V we describe the problem with the NERI and introduce our solution. Section VI presents experimental results and the paper is concluded in section VII.

II. SwissRanger SR-3000

The state-of-the-art range camera SR-3000 [8], [10] is developed and manufactured by MESA Imaging. It is a CMOS sensor and consists of 176 × 144 Focal Plane Array (FPA) sensors/pixels. The FPA enables capturing a 3D scene with a spatial resolution of 176 × 144 pixels at video frame rates. The FPA is also referred to as image plane, since it can be represented as a digital image. The camera has a physical dimension of 50 mm × 48 mm × 65 mm and a field of view of 47.5 × 39.6 degrees. It uses 55 infrared LED (wavelength: 850 nm) for illumination. The light source is amplitude modulated. The camera can be operated in four modes with different modulation frequency (19MHz, 20MHz, 21MHz and 30 MHz) which also determines the non-ambiguity range. In our case a modulation frequency of 20MHz is used and the non-ambiguity range is 7.5 meters. The sensor's current technology restricts its use within indoor environments.

A. Operating Principle:

The SR-3000 performs range measurement by indirect Time-Of-Fight (TOF). Fig. 3 illustrates the TOF measurement taking place in a single FPA pixel. The emitted amplitude modulated light is reflected by the object surface and received by the sensor. The received signal at each pixel is then demodulated to reconstruct the incoming signal. The phase shift between the emitted and reconstructed signals is measured. The distance between the object's surface and the sensor can be determined by the phase shift. Each range measurement of the sensor is translated from spherical coordinate to Cartesian coordinate and converted to a 3-D data point (with X, Y and Z coordinate values). This results in a set of 176×144 data points for each captured frame. The camera uses the offset between the emitted and received signals to determine the intensity information. Hence it delivers both intensity and range images for each captured frame.

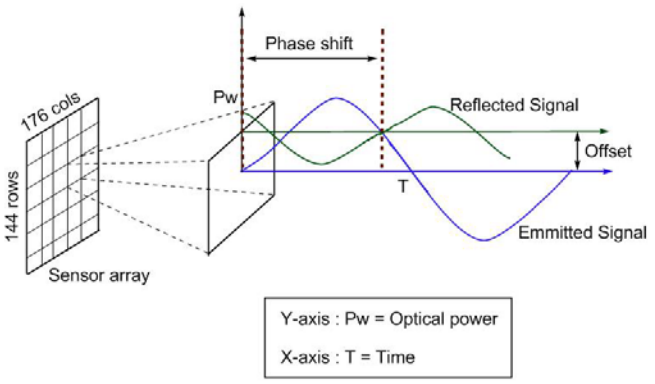

Fig. 3 TOF measurement in a FPA pixel

The sensor's error in range measurement is affected by various environmental factors such as surface reflectivity and target distance in addition to the intrinsic factors such as noise of the CMOS sensor and driving electronics. The details on the effect of these factors can be found in [12]. The intent of

this paper is not to correct the sensor's measurement error, but address the possibility of reducing the effect of the error on range data processing.

III. SVD Filter for Image Reconstruction and Noise Reduction

A. Image Reconstruction

SVD and Eigen vector analysis are classical tools used in digital image processing [13]. An $M\times N$ image can be denoted by matrix $\mathbf{A}= [a_{ij}]$ for i=1, …, M and j=1, …, N. The SVD of matrix **A** takes the following form:

$$\mathbf{A} = \mathbf{USV}^T = \sum_{i=1}^{R} \mathbf{u_i} s_i \mathbf{v}_i^T , \quad (1)$$

where the orthogonal matrices **U** and **V** consists of the left and right singular vectors $\mathbf{u_i}$ and $\mathbf{v_i}$, i.e., $\mathbf{U}=(\mathbf{u_1}, ..., \mathbf{u_M})$ and $\mathbf{V}=(\mathbf{v_1}, ..., \mathbf{v_N})$. **U** and **V** are of order $M\times M$ and $N\times N$, respectively. **S** is a $M\times N$ matrix where the diagonal elements s_i are the nonnegative singular values of **A** and all off-diagonal elements are zero. s_i are arranged in a nonincreasing order, i. e., $s_1 \geq s_2 \geq \ldots\ s_R \geq 0$, in matrix **S**. If the rank of **A** is $R \leq min(M, N)$, then $s_i > 0$ for i=1, …, R and s_i=0 for i=R+1, …, N. The SVD of **A** indicates that an image can be restored as the weighted sum of a set of base images $\mathbf{E_i} = \mathbf{u_i v_i^T}$ for i=1, …, R. Each base image is also called an Eigen image because the singular value is the square root of the corresponding Eigen values of $\mathbf{A^TA}$ [14]. The singular value s_i represents the contribution of the i^{th} base image to the reconstruction of image **A.** The decreasing order of s_i in matrix **S** implies that the i^{th} base image's contribution decreases as i approaches R. Although a large number of Eigen images are required for an accurate reconstruction of an image, a smaller number of Eigen images are generally sufficient to represent the image. This property is exploited in image compression and coding techniques. Below is an illustration explaining an image reconstruction process. Fig. 4(a) is the snapshot of the scene for the case study that consists of a cardboard. The intensity image of the scene is obtained by the SR-3000 camera. For an illustration purpose, the SVD is performed over this image. Since the SR-3000 camera has spatial resolution of 176×144 pixels, the SVD process results in 144 base images. Figure 4(b)-4(g) shows six reconstructions, each of which has a different Number of Base Images (NBI) and file size (in Kilobyte) of the resultant image. Apparently, Fig. 4(g) is the SR-3000's raw intensity image since it contains all of the 144 base images. From the illustration we can see that image reconstruction is not possible with too fewer base images due to excessive loss of image information. However, using too many base images may result in an unnecessarily large file size but does not improve image quality a lot. A close examination of Fig. 4(d) and Fig. 4(e) reveals that the NBI increment actually adds noise into the image. This suggests that a high quality image (less noisy and with a smaller file size) can be obtained by using a suitable NBI.

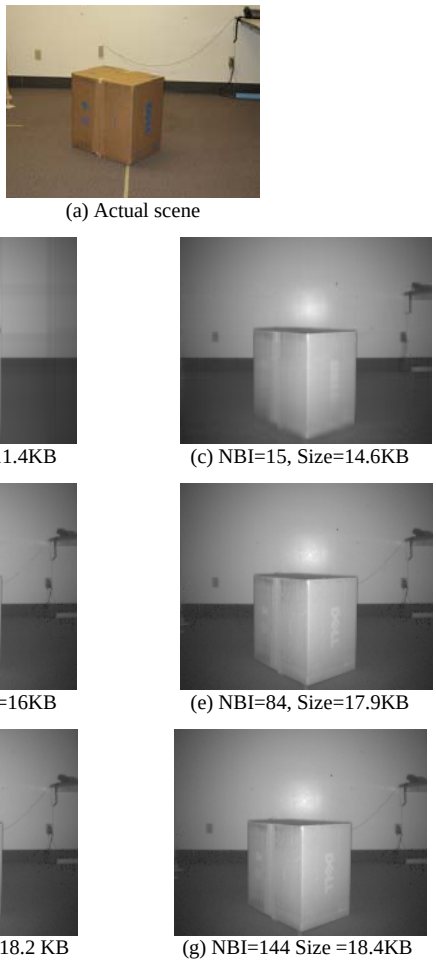

(a) Actual scene

(b) NBI=3, Size=11.4KB

(c) NBI=15, Size=14.6KB

(d) NBI=45, Size=16KB

(e) NBI=84, Size=17.9KB

(f) NBI=120, Size=18.2 KB

(g) NBI=144 Size =18.4KB

Fig. 4 Image reconstruction using different NBI: the image with NBI=45 is satisfactory in term of the noise level and file size.

B. SVD Filtering

The SVD technique is also used to filter noise for a given set of data or image. A noise-free image **A** has a lower rank ϵ, $\epsilon < min\ (M, N)$ [15]. The SVD in Eq. (1) produces the following singular values in a nonincreasing order: $s_1 \geq s_2 \geq s_3 \geq \ldots \geq s_\epsilon > s_{\epsilon+1} = \ldots = s_{min(M,N)} = 0$. A noisy image can be described by matrix $\mathbf{B}=\mathbf{A}+\mathbf{E}$, where **E** is a noise perturbation matrix. Matrix **B** has a full rank $R=min(M, N)$ [15]. This means that the last R-ϵ base images are additive noise. By eliminating the singular values $s_{\epsilon+1}, \ldots, s_R$, we may remove the noise but preserve the image details.

Figure 5 pictorially describes different components of a noisy image from a singular value perspective. As mentioned above, there exist a certain number of singular values that signify image components and the remaining singular values represent noise.

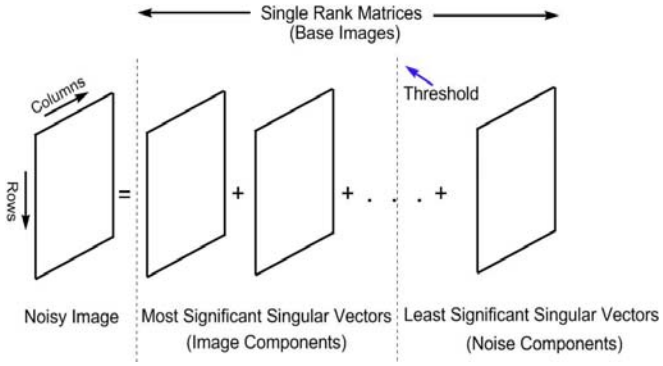

Fig. 5 Pictorial representation of image reconstruction

This can be qualitatively demonstrated by the example in Fig. 6 where the Sobel edge detector is used to identify the edges—the most distinctive features—of the image. Figure 6(a) is the snapshot of the scene. The intensity image of the scene (Fig. 6(b)) is obtained from the SR-3000. The reconstructed intensity images with the first ten singular values and the last forty singular values are shown in Fig. 6(b) and Fig. 6(d), respectively. The corresponding edge images, obtained by the Sobel edge detector, are depicted in Fig. 6(c) and Fig. 6(e). It can be seen that Fig. 6(d) mostly represents noise (no signal component) whereas Fig. 6(b) mostly consists of the signal components (with a very low noise level).

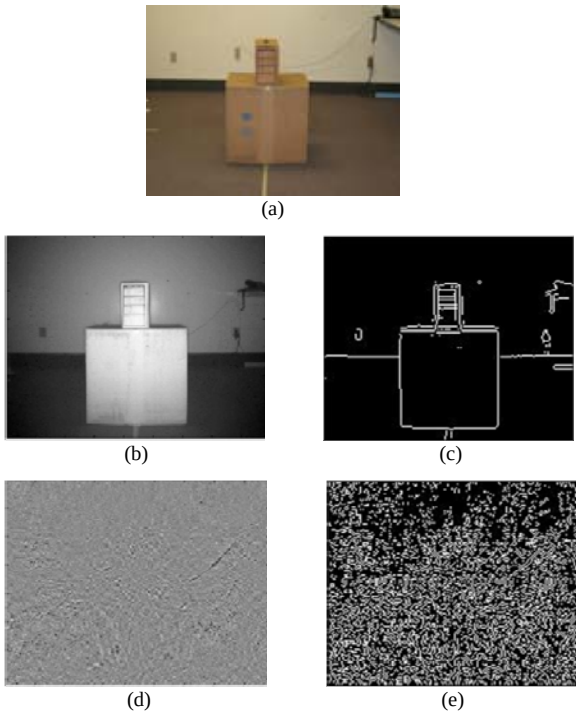

Fig. 6 A qualitative demonstration of the correlation between the image and the significant singular values, and the correlation between the noise and the insignificant singular values: (a) Actual Scene, (b) Intensity Image with the first ten singular values, (c) Edge image of (b), (d) Intensity image with the last forty singular values, and (e) Edge image of (d).

In order to implement the above SVD filtering technique, an optimal value of ϵ must be determined. In [15] a block-based SVD filtering method is proposed to remove noise in an intensity image. The method exploits the fact that random noise is hard to compress whereas image (ordered information) is not, and it determines the optimal value of ϵ by the following procedures: (1) reconstruct an intensity image using Eq. (1) with the last k singular values nullified; (2) perform a lossless compression on the resultant image and record the image file size $F(k)$; (3) perform steps (1) and (2) from k=1 until k=R and plot $F(k)$ against log(k); (4) find the knee point of the curve (where the second derivative reach its maximum) and ϵ locates at the knee point. In [16] a similar approach is used to filter random noise from deterministic data.

IV. Problem Description

Edge information of an intensity image plays an important role in image segmentation. An edge indicates a large variation of intensity in the neighboring pixels which may be related to a variation in surface normal. Many researchers [19], [20], [21] have used edge information to serve an image segmentation process for various applications. It is logical to think that the edges of SR-3000's intensity image may be helpful to range image segmentation. However, we use only the range image in this study due to two reasons: (1) The quality of the SR-3000's intensity images is not good; and (2) An edge of the intensity image does not always relate to a change in surface normal. The pattern/texture of a surface or shadows may also be detected as edges.

Since a range image encodes depth information as grey level, edges of an object may be indistinctive. This can be seen in Fig. 7(b). For proper segmentation, the edges need to be enhanced. A typical enhancement method is to encode each pixel's grey level using its surface normal and depth information [18]. This method is adopted in this study and will be detailed in Section V. Figure 7(c) shows the Normal-Enhanced Range Image (NERI). One can see that the edges are much more distinctive in the NERI, but the surfaces are corrupted at the same time. The corruption is caused by the range errors that create variations of surface normal. The level of corruption can be qualitatively evaluated by the edge image in Fig. 7(d) that is extracted by using the Sobel detector. The edge image consists of many tiny irregularities in addition to the object's edges. It is apparent that such an edge image is in no way helpful to range image segmentation. We have attempted to use the SVD filtering method [15], [16] to reduce the corruption in the NERI. It is found that the SVD filter itself works very well but the method proposed in [15], [16] for determining the threshold ϵ does not work. We suspect that it is because the corruption is not merely caused by random noise in our case.

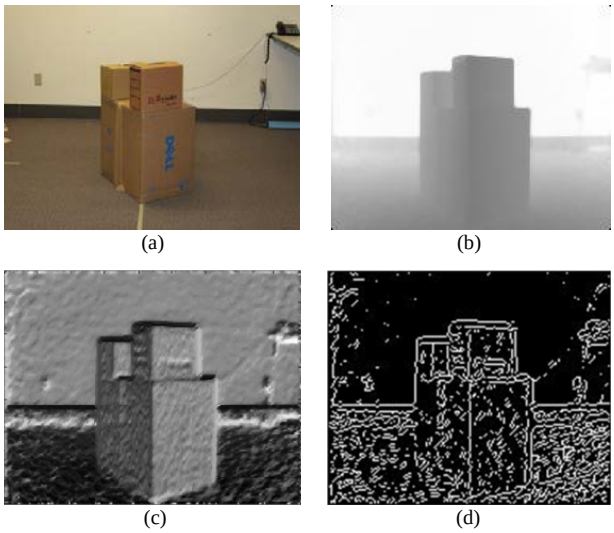

Fig. 7 Conventional range image vs NERI: (a) Actual scene, (b) Range image of the scene, (c) NERI, and (d) Edge image of (c).

Based on our experiments on a large number of different environments, we find that it is possible to determine the threshold ϵ for the SVD filter by simply analyzing the singular values. The SVD filter with such ϵ works pretty well. Unlike the method in [15], [16], our approach does not need to analyze the reconstructed images and is thus very computationally efficient.

V. The Proposed Method

As we have seen in section IV that the value of ϵ determines the quality of the reconstructed image. A good estimation of ϵ should result in a reconstructed image where most of the image features are retained and the majority of the noise is eliminated. In this section, we describe how we construct the NERI and choose an appropriate value for ϵ.

We first construct a tri-band color image [17], [18] where each pixel's RGB values are encoded using the x and y components of its surface normal and its depth information. The tri-band image is converted to a gray image, i.e., the NERI. We then perform the SVD, i.e., Eq. (1), on the NERI. Since the matrix of the NERI is 176×144 and has full rank due to noise, we have 144 singular values s_i for i=1,…,144 that are arranged in nonincreasing order. The plot of s_i against i shows that the singular values drop drastically with increasing i. The curve stays flat when i is sufficiently big. In other words, the first derivatives of the singular values initially have negatively big values, and they rapidly approach to zero as i increases. This property holds true in all of our experiments with various scenes and it suggests that we may readily choose the value ϵ by setting a threshold to the curve of the first derivative.

Our SVD filtering method is carried out as follows:

1) Construct the NERI and obtain the singular values, s_i for i=1,…,144, of NERI matrix.
2) Normalize s_i by $\bar{s}_i = s_i / \max(s_i)$ and compute the first derivatives $\bar{s}_i' = d\bar{s}_i / di = d\bar{s}_i$ for i=1,…,143.
3) The first singular value $\bar{s}_K'$ in $\bar{s}_i'$ (i=1,…,143) that satisfies $\bar{s}_K' > \delta$ is recorded, where δ is a threshold empirically determined through experiments. δ=0.001 in this study. The threshold value for the SVD filter is then determined as $\epsilon=K+1$.
4) Set the last 144-ϵ singular value to zero, i.e., s_i=0 for $i=\epsilon+1,\ldots,144$; and reconstruct the NERI using Eq. (1).

VI. Experimental Results

A. Hardware and Software Setup

Our experimental setup is depicted in Fig. 8. The tripod-mounted SR-3000 is connected to a Sony Vaio–SZ220B laptop through a USB 2.0 interface. The laptop is powered by a 1.83GHz Intel Core Duo processor and uses Windows XP as OS. We use MATLAB 7.0 and the SR3000's Matlab library to acquire sensor data.

Fig. 8 Hardware setup

B. Results

As the camera is designed for indoor use, we concentrate our experiments in representative indoor environments. We first describe the different stages of the proposed filtering method using the example in Fig 9, and then validate the method with numerous experiments.

We carry out our first experiment in the environment as depicted in Fig. 9(a). The tri-band color image and the NERI are shown in Fig. 9(b) and Fig. 9(c), respectively. To further explain the principle of our SVD filtering method, the curve of s_i versus i is plotted in Fig. 10. We can see a sharp decrease in the magnitude of the first few singular values. In this example the most significant singular value is 19922 and the least significant singular value is 7. The plot of the first derivatives of the singular values is shown in Fig. 11. We can observe that the values of the first derivatives approach to zero rapidly. The values may oscillate in a narrow range in the

vicinity of zero (Fig. 12) but the overall trend is moving towards zero. It is noted that the curves are plotted using the actual singular values to show their true magnitudes. By using a threshold value of -20 (0.001 if normalized), the value of ϵ is determined to be 12 (see Fig. 12). The filtered NERI is shown in Fig. 9(e), which is much smoother than Fig. 9(c). The filtered NERI still has distinctive edges for each object. The enhancement of image quality can also be verified by comparing the edge image in Fig. 9(f) with that in Fig. 9(d).

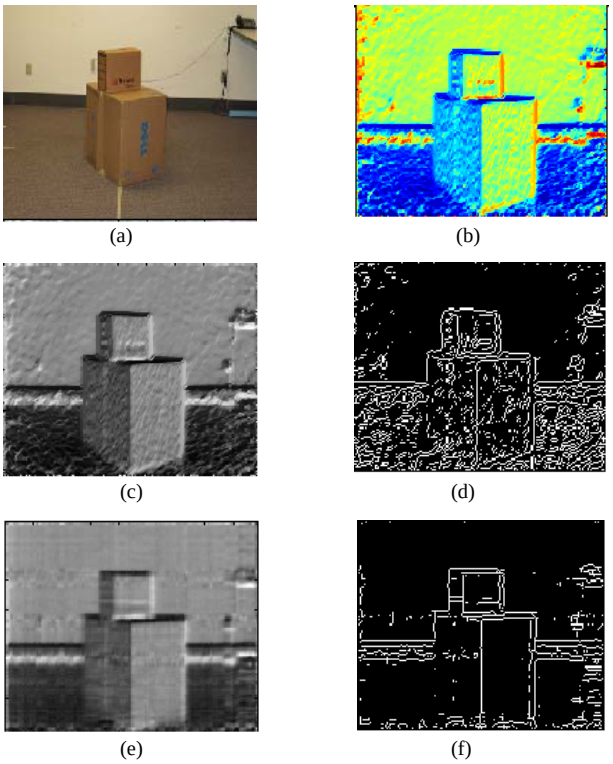

Fig. 9 Experiment one: (a) Actual scene, (b) Tri-band color image, (c) Original NERI, (d) Edge image of (c), (e) Filtered NERI (ϵ=12), and (f) Edge image of (e).

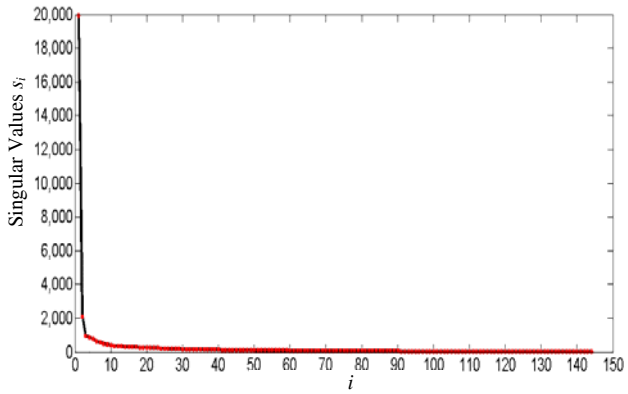

Fig. 10 Plot of the singular values

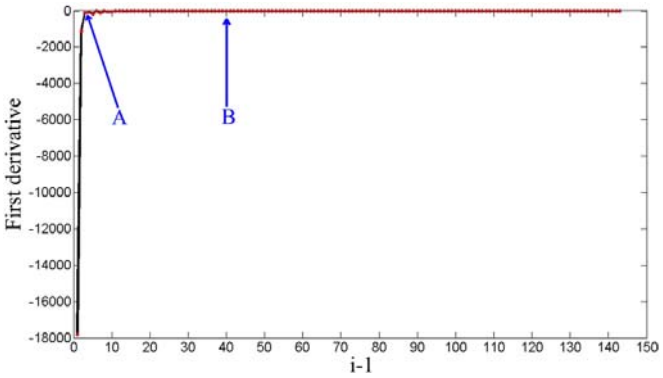

Fig. 11 Plot of the first derivatives of the singular values

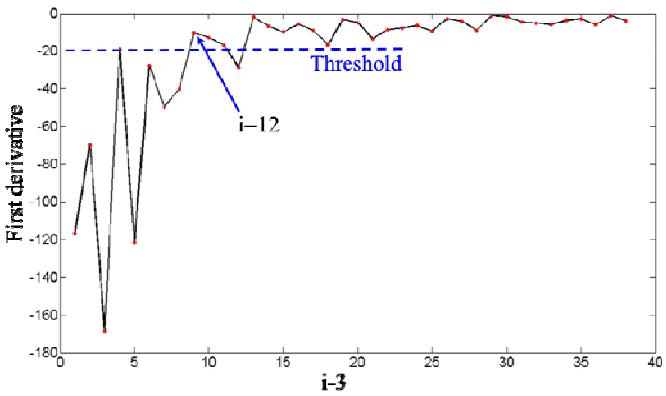

Fig. 12 Magnified view of segment AB.

Fig. 13 shows the experimental results in an environment consisting of 4 vertical sticks. The number of effective singular values (i.e., the value of ϵ) is found to be 9. The values of δ used in this and subsequent experiments are the same (δ=0.001). The Sobel edge detector with a threshold value of 8 is used to obtain the edge images in all our experiments to qualitatively show the degree of corruption before and after the filtering method is applied. The threshold values ϵ obtained by this and the subsequent experiments are listed in Table I.

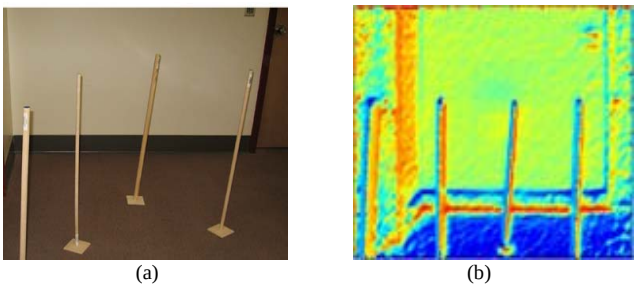

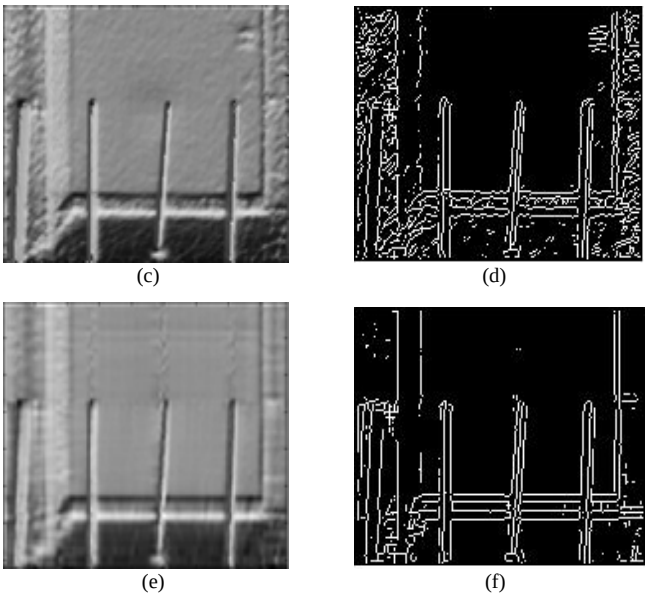

(c) (d) (e) (f)

Fig. 13 Experiment two: (a) Actual scene, (b) Tri-band color image, (c) Original NERI, (d) Edge image of (c), (e) Filtered NERI (ϵ=9), (f) Edge image of (e)

Our next case study is implemented in an environment with a trash can. The targeted application could be automatic waste disposal systems, wherein a mobile robot is used to locate a thrash can. Figure 14 shows the experimental results.

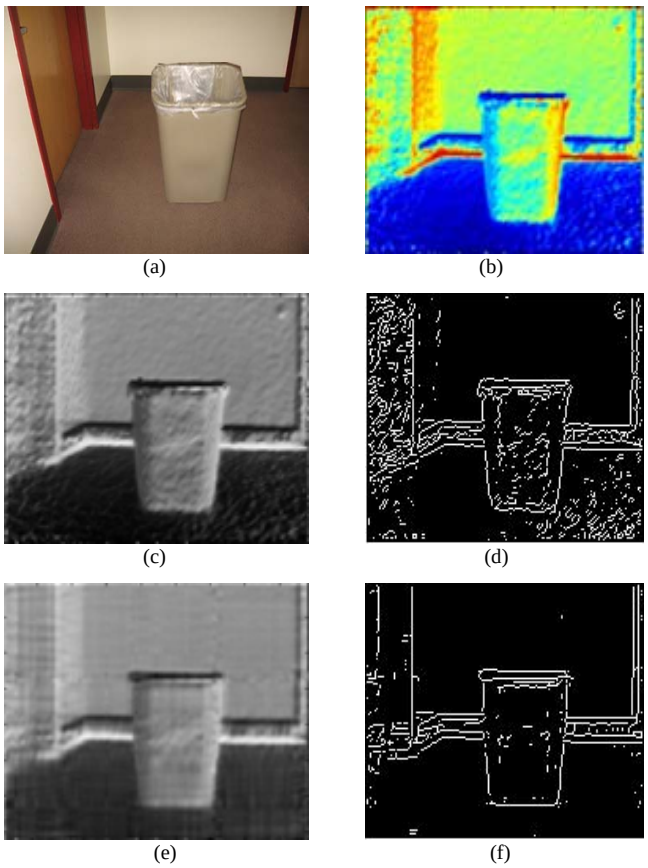

(a) (b) (c) (d) (e) (f)

Fig. 14 Experiment three: (a) Actual scene, (b) Tri-band color image, (c) Original NERI, (d) Edge image of (c), (e) Filtered NERI NERI (ϵ=12), and (f) Edge image of (e)

Experiment four is conducted on a cluttered environment consisting of a shelf and toolbox rack. The results are shown in Figure 15.

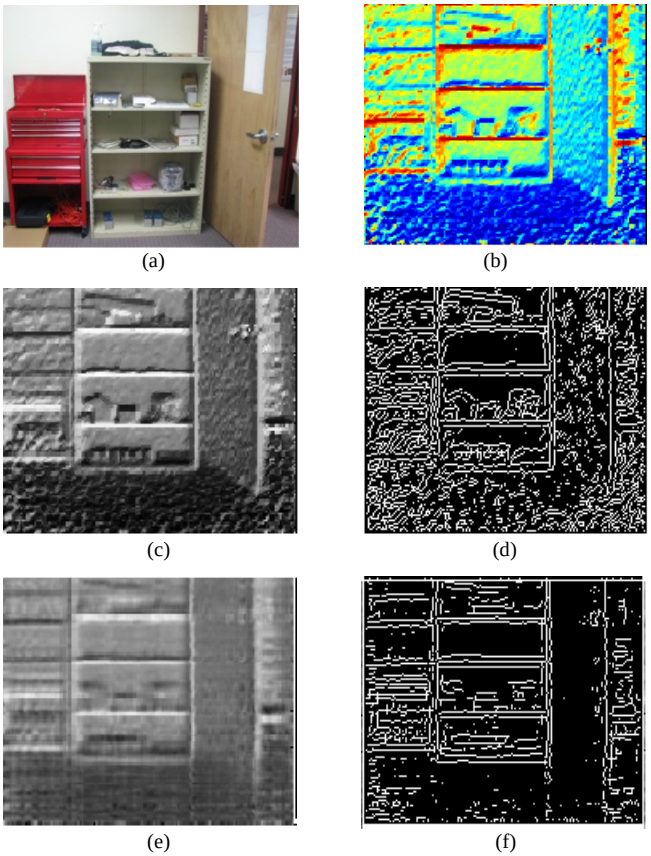

(a) (b) (c) (d) (e) (f)

Fig. 15 Experiment four: (a) Actual scene, (b) Tri-band color image, (c) Original NERI, (d) Edge image of (c), (e) Reconstructed NERI (ϵ=7), and (f) Edge image of (e)

Experiments five and six validate the method in the cases of stairways (Fig. 16) and hallway (Fig. 17).

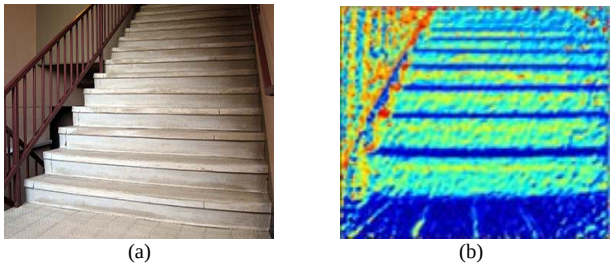

(a) (b)

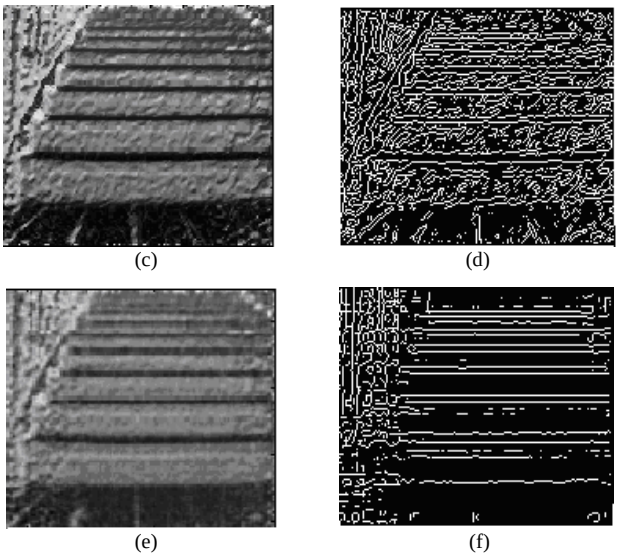

Fig. 16 Experiment five: (a) Actual scene, (b) Tri-band color image, (c) Original NERI, (d) Edge image of (c), (e) Filtered NERI (ϵ=8), (f) Edge image of (e)

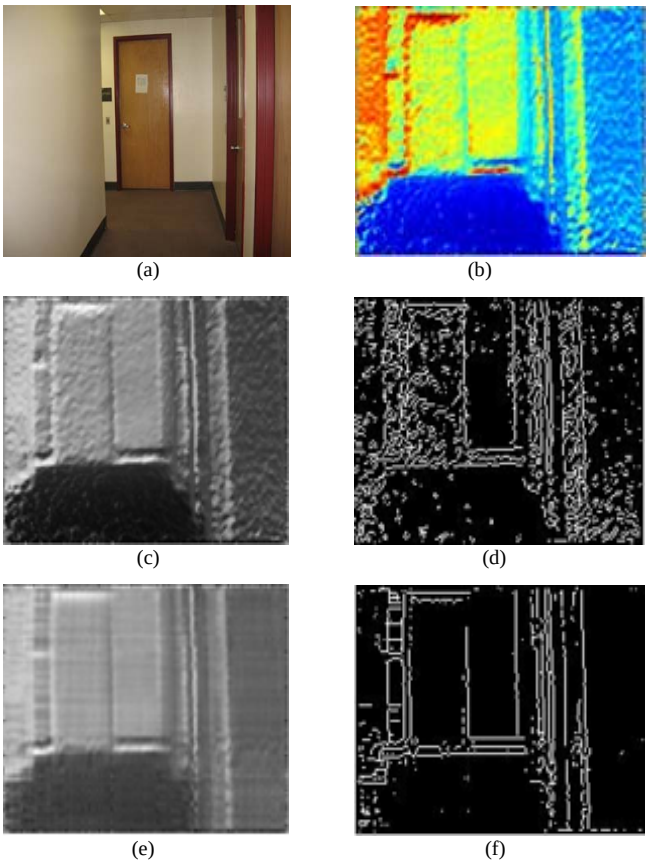

Fig. 17 Experiment six: (a) Actual scene, (b) Tri-band color image, (c) Original NERI, (d) Edge image of (c), (e) Filtered NERI (ϵ=10), and (f) Edge image of (e)

Table I summarizes the results of the five experiments that indicate: (1) A small number of base images are sufficient for reconstructing a NERI; (2) The filtering method is computationally inexpensive. It should be noted that the computational time can be substantially reduced if we would write the code in C++.

TABLE I SUMMARY OF THE EXPERIMENTAL RESULTS

Scene	Figure	Maximum SV	Threshold ϵ	Time (seconds)
Sticks	13	21830	9	0.969
Thrash can	14	19556	12	0.98
Shelf	15	18729	7	1.3
Staircase	16	17361	8	1.8
Hallway	17	18391	10	0.938

SV: Singular Values

VII. Conclusions And Future Work

We have presented a method to enhance the SwissRanger SR-3000's range images. The method first converts a conventional range image into a Normal-Enhanced Range Image (NERI) where each pixel's intensity is encoded by x and y components of the surface normal and the depth information of the corresponding pixel in the conventional range image. The NERI enhances the objects' edges but corrupts their surfaces due the noise in the range data. We have developed a SVD filtering method to reduce the corruption and preserve the details of the NERI. Our experiments show that the technique can effectively filter the noise in the range data with no prior knowledge of either the range image or noise characteristics. The filtering method is computationally inexpensive and thus suitable for real-time applications. In our future work we plan to investigate into the fundamental aspects of the SVD filter from the perspective of the NERI enhancement.

References

[1] C. Ye, "Navigating a mobile robot by a traversability field histogram," *IEEE Transactions on Systems, Man, and Cybernetics-Part B: Cybernetics*, vol. 37, no. 2, pp. 361-372, 2007.

[2] R. Turchetto and R. Manduchi, "Visual curb localization for autonomous navigation," in *Proc. IEEE/RSJ International Conference on Intelligent Robots and Systems*, 2003, pp. 1336-1342.

[3] http://www.3dvsystems.com

[4] http://www.canesta.com

[5] R. Stettner, H. Bailey, and R. D. Richmond, "Eyesafe laser radar 3d imaging," in *Proc. SPIE*, vol. 4377 of *Laser Radar Technology and Applications*, 2001.

[6] R. Gvili, A. Kaplan, E. Ofek and G. Yahav, "Depth key," in Proc. *SPIE Electronic Imaging Conference,* Santa Clara, California, 2003.

[7] S. B. Gktürk, H. Yalcin, and C. Bamji, "A time-of-flight depth sensor system description, issues and solutions," in *Proc. IEEE Computer Society Conference on Computer Vision and Pattern Recognition Workshops*, 2004, pp. 35-35.

[8] T. Oggier, B. Büttgen,F. Lustenberger, "SwissRanger SR3000 and first experiences based on miniaturized 3D-TOF Cameras," *Swiss Center for Electronics and Microtechnology, CSEM, IEE, Fachhochschule Rapperswil Switzerland, Technical Report, 2005*

[9] C. Ye and J. Borenstein, "Characterization of a 2-D laser scanner for mobile robot obstacle negotiation," in *Proc. IEEE International Conference on Robotics and Automation*, 2002, pp. 2512-2518.

[10] T. Oggier, *et al.*, "An all-solid-state optical range camera for 3D real-time imaging with sub-centimeter depth resolution," in *Proc. SPIE*, vol. SPIE-5249, 2003, pp. 534-545.

[11] M. Lehmann, R. Kaufmann, F. Lichtenberger, B. Büttgen and T. Oggier, "CCD/CMOS lock-in pixel for range imaging: Challenges, limitations and state-of-the-art," in *Proc. 1st Range Image Research Day*, 2005, pp. 21–32.
[12] S. A. Guðmundsson, H. Aanæs, and R. Larsen, "Environmental effects on measurement uncertainties of time-of-flight cameras," in *Proc. International Symposium on Signals Circuits and Systems*, July 2007, pp. 1-4.
[13] H. C. Andrews and C. L. Patterson, "Singular value decompositions and digital image processing," *IEEE Transactions on Acoustics, Speech, and Signal Processing,* vol. ASSP-24, pp. 26–53, 1976.
[14] D. C. Lay, *Linear Algebra and its applications*, 2nd ed., Addison Wesley Longman, Inc, April 2000.
[15] K. Konstantinides, B. Natarajan, and G. S. Yovanof, "Noise estimation and filtering using block-based singular value decomposition," *IEEE Transactions On Image Processing,* vol. 6, no. 3, pp. 479-483, 1997.
[16] B. K. Natarajan, "Filtering random noise from deterministic signals via data compression," *IEEE Transactions on Signal Processing*, vol. 43, no.11, pp. 2595–2605, 1995.
[17] K. Pulli, M. Pietikainen, "Range image segmentation based on decomposition of surface normals," in *Proc.* 8th *Scandinavian Conference on Image Analysis,* vol. 2, pp. 893-899, 1993.
[18] K. Pulli, "Vision methods for an autonomous machine based on range imaging," Master's Thesis, University of Oulu.
[19] Y. Zhang, Y. Sun, H. Sari-Sarraf, and M. A. Abidi, "Impact of intensity edge map on segmentation of noisy range images," in *Proc. SPIE Conference on Three Dimensional Image Capture and Applications III*, 2000, pp 260-269.
[20] T. Pavlidis, and Y. T. Liow, "Integrating region growing and edge detection," *IEEE Transactions on Pattern Analysis and Machine Intelligence*, vol. 12, no.3, pp. 225-233, 1990.
[21] J. L. Moigne, J. C. Tilton, "Refining image segmentation by integration of edge and region data," *IEEE Transactions on Geoscience and Remote Sensing*, vol. 33, no. 3, pp. 605-615. May 1995.
[22] Y. M. Kim, D. Chan, C. Theobalt, and S. Thrun, "Design and calibration of a multi-view TOF sensor fusion system," *IEEE Computer Society Conference on Computer Vision and Pattern Recognition Workshops, 2008.* pp. 1 – 7.

Guruprasad M Hegde received B.E. degree from Sardar Vallabhbhai National Institute of Technology, India in June 2005. He is currently working towards a PhD in Engineering Science and Systems at the University of Arkansas at Little Rock, AR. He is a student member of IEEE and his current research interests include range image segmentation and robot navigation.

Cang Ye received B.E. and M.E. degree from the University of Science and Technology of China, P. R. China in 1988 and 1991, respectively. He received his Ph.D. degree from the University of Hong Kong in 1999.

He is currently an Assistant Professor in Department of Applied Science, University of Arkansas at Little Rock, AR. He was a research investigator at University of Michigan, Ann Arbor, MI from 2003 to 2005. His research interests are in mobile robot terrain mapping and navigation, fuzzy systems and reinforcement learning.

Dr. Ye is a senior member of IEEE and a member of Technical Committee on Robotics and Intelligent Sensing, IEEE Systems, Man, and Cybernetics Society.